MOSFET Junction Temperature Measurements using Conducted Electromagnetic Emissions and Support Vector Machines

Justin Demus[+], Viktoriia Sysoeva, Qianyi Cheng, Matt Boubin, Ahmed Siraj, Mark Scott*
Department of Electrical and Computer Engineering
Miami University
Oxford, OH U.S.A.
[+]: demusjc@miamioh.edu
*: scottmj3@miamioh.edu

***Abstract*—As power electronics permeate critical infrastructure in modern society, more precise and effective diagnostic methods are required to improve system reliability as well as reduce maintenance costs and unexpected failures. Prognostic and Health Management (PHM) systems that analyze changes in the electromagnetic spectrum (E-PHM) of a circuit can be implemented to determine the health of the equipment under test. This research demonstrates the use of E-PHM techniques to measure the junction temperature of a silicon carbide (SiC) MOSFET. The results show the feasibility of training machine learning algorithms to recognize this relationship and determine the junction temperature within 10 °C. This is accomplished, in situ, without interruption of device operation and without altering the system's performance.**

Keywords—electromagnetic interference, prognostic and health management, E-PHM, machine learning, support vector machine, junction temperature measurements.

I. Introduction

It is increasingly necessary to improve the reliability of power electronics because they are now found in numerous safety-critical operations wherein hardware failure yields serious consequences [1], [2]. Within high-power applications, like electrified transportation, power electronics drive substantial loads at high voltages for sustained periods of time under a wide range of environmental stresses, making them liable for failure [3]. High costs are associated with preventing failure, accentuated by a lack of device monitoring tools. For example, the airline industry resorts to ambiguous testing and preventative maintenance for their aircraft due to the absence of accurate diagnostic procedures; this contributes to a 10% to 20% rise in maintenance costs [4]. Improvements to monitoring systems can help mitigate these issues.

Prognostic and Health Management (PHM) systems are real-time analysis hardware that draw on background knowledge of a device's operational characteristics and failure mechanisms to ascertain the health of the device. This area of research has grown considerably with respect to the field of power electronics since this hardware is becoming ubiquitous to many mission critical applications. While several variants of PHM methods have been explored for power electronics, the use of electromagnetic interference (EMI) as a conditional monitoring tool, referred to as E-PHM, has received limited attention [3] - [6] despite its utility as a sensitive and non-invasive insight into circuit operation.

Effective implementation of PHM techniques depends on the complex task of linking device behavior to internal characteristics indicative of incipient device failure. Typically, power device testing and datasheets lack sufficient detail to effectively model the relationship between internal operation and external behavior; for example, device behavior is often characterized at only two different temperatures, omitting details of the complex nonlinear relationship and the full extent of its effects on device operation. Semiconductor operating characteristics are sensitive to changes in temperature, altering several properties and behaviors. Analysis of temperature dependent characteristics by several other researchers concludes that on-state resistance ($R_{DS(on)}$) and switching speed (both turn on and turn off) are all altered according to the device temperature [7]-[9]. The latter is due to changes in the threshold voltage and mobility [9]. These temperature-dependent changes in circuit behavior are reflected in the electromagnetic (EM) spectrum of the circuit [10]. This research quantifies the accuracy of using changes in conducted EMI to determine device junction temperature of a switching device via the use of support vector machines (SVMs).

This paper discusses the topology used to generate EMI and the measurement techniques used to gather data. Experimental data is provided, with key features in the EMI emphasized. Following these results, the implementation of the SVM learning algorithms is discussed. The paper then delivers final conclusions and discussions of future work to be conducted.

II. Background

Datasheets for most power devices include only basic information concerning how temperature affects different aspects of operational characteristics. In the context of this research, characteristics such as switching speed and $R_{DS(on)}$ are of key importance as their effects on EMI are likely to distinguish noise measurements between different device junction temperatures. Several studies have been released which provide a closer analysis of temperature dependent SiC MOSFET characteristics. Characterization of devices is typically accomplished in these studies through the development of a converter topology and a series of double pulse tests (DPT),

978-1-7281-0395-2/19/$31.00 ©2019 IEEE

each topology analyzed with the switching device heated to various temperatures. Furthermore, these studies characterize multiple semiconductor materials, including Si and SiC, to compare the relative performance of each material at several temperature ranges. The results of these studies indicate that multiple device characteristics are liable for alteration when subjected to different temperature, even during device operation. Exploitation of these distinguishing characteristics - which include altered switching losses, switching speeds, and adjusted gate voltage curves – allows for a distinction in the EMI signature of these devices. This section seeks to correlate the results of these past analyses to an expected shift in the EMI spectrum of a SiC device.

A. Static Characterization

Analysis by past researchers has concluded through both static and dynamic characterization of semiconductor devices that temperature can significantly impact a device's function. [9] features a plot of threshold voltage versus temperature indicating a clear negative temperature coefficient across all tested SiC devices, concluding that an increase in device temperature alters the conditions necessary for turn-on in these MOSFETs. Subsequent analysis of these devices indicates a decisive shift in transconductance when comparing device operation at 25 when compared with 200 . Such a dramatic shift in transconductance implies a reduced turn-on time, potentially indicating a proportional shift in EMI with respect to temperature.

Further evidence suggests that switching speed is affected by junction temperature: drain voltage and drain current slew rates were shown to increase with temperature [7]. Changes in switching characteristics can be observed in the circuit's EMI as well. Xiang et al. [2] determined a 15 change in case temperature yielded a 5.6 % change in fifth harmonic currents as a result of temperature-dependent switching speeds, proving the efficacy of corroborating EMI to device temperature.

Finally, a relationship between $R_{DS(on)}$ and device junction temperature is explored at length by many researchers, both through experimentation and simulation. LTSpice device simulations based on the VDMOS model were developed to incorporate realistic parasitic effects and temperature dependent models with the goal of estimating changes to current transient properties [12]. These simulations yielded a positive temperature coefficient for $R_{DS(on)}$. Subsequent experiments by [13] indicated an increase in $R_{DS(on)}$ coupled with a decrease in threshold voltage. These results are supported by [9], this time applied to a wide selection of SiC and Si devices for comparison. In their test setup, $R_{DS(on)}$ for multiple SiC and Si devices was extracted from I-V curves at various temperatures and multiplied by the respective die area to achieve the device's specific on resistance. $R_{DS(on)}$ for all devices followed a similar gradual increase as the temperature was raised. A comparison of Si MOSFETs with their SiC counterparts reveals a more substantial increase in $R_{DS(on)}$ for the Si devices (with an increase of over 100%), though both types of devices still revealed a noteworthy rise. An increase in device temperature gradually diminishes the current gain of a MOSFET (indicating increased $R_{DS(on)}$), as elevated temperature raises drift region resistance [8]. These results are corroborated by [10] through similar experimentation with another set of semiconductor devices. Again, both Si and SiC devices exhibit a consistently increasing resistance as temperature rises, with Si subject to far greater losses.

Increased $R_{DS(on)}$ in a switch will naturally lead to increases in conductive energy losses as the device heats up, confirming the theory that energy losses can reliably predict device temperature during device operation. Qi et al. [10] divides the total $R_{DS(on)}$ into channel resistance (R_{CH}) and all remaining components (R_S) and attributes the temperature specifically to shifts in R_{CH}. At higher temperatures, R_S dominates the $R_{DS(on)}$ due to bulk electron mobility. In contrast, R_S diminishes at low temperatures as bulk electron mobility subsequently increases. Additionally, R_{CH} begins to rise as the device cools predominantly according to an increase in trapped electrons (among other less prevalent factors) [11]. Chen et. al. [6] reaches the same conclusion, determining that the shifts in I-V curves as temperature increases reflects a proportional shift in energy losses by each device.

B. Dynamic Characterization

Switching characterization of the circuits was accomplished using a standard double pulse test. A constant ambient temperature is maintained while a heating apparatus (e.g. a hotplate or a heat source mounted on the device) actuates the temperature of the devices as double pulse tests are conducted.

DPT tests conclude that a substantial increase in switching loss occurs as device temperature increases [1], [7], [9], [11]. As predicted, Si device losses far exceed that of the SiC devices, again demonstrating the efficacy of these improved SiC devices. Nevertheless, the switching losses are still observable on an easily measurable scale, with turn-off energy (E_{OFF}) increasing with respect to temperature and turn-on energy (E_{ON}) decreasing. These changes are a consequence of the temperature dependent switching speeds discussed in the previous section. Plots in these papers repeatedly show a decrease in turn-on time, revealing the source of the reduction in E_{ON}. Likewise, [10] depicts a clearly observable increase in turn-off time as temperature increases, corroborating the increase in E_{OFF}.

C. Machine Learning

The development of machine learning algorithms has facilitated the rise of efficient and versatile data processing tools that can be implemented with relative ease in many industrial and scholarly applications. Support vector machine (SVM) modeling is predicated on the establishment of decision planes to categorize input data into predefined classes. This decision plane is represented mathematically as a hyperplane, wherein data from a given input vector is mapped to a "feature space" via a kernel function designated by the user. Once the input data item (known as a "feature"), has been mapped into the feature space, the SVM creates an optimal decision line within the hyperplane that separates data into each respective class [14].

The number of classes and characteristics of each class are defined according to a training model introduced to the machine prior to data processing. This training model is comprised of labeled data samples used by the SVM algorithm to create the hyperplane responsible for separating input data. Creation of the

hyperplane is carried out by a desired kernel function, most popularly the radial basis function (RBF). This function is described as follows:

$$K(x, x_i) = exp\left(\frac{-\gamma|x-x_i|^2}{\sigma}\right) \quad (1)$$

wherein x describes the class, x_i represents a data set, σ indicates the standard deviation of the data set, and γ acts as a scalar.

Having established the classifier according to the training model, an unsupervised input data vector is compared to the hyperplane. This comparison is described according to the following equation:

$$f(x) = \sum_{i=0}^{N} a_i y_i K(x, x_i) + b \quad (2)$$

wherein a_i describes a scaling factor, y_i represents the input vector, and b is the error offset constant. This process is repeated for each member of the input vector.

In the context of this experiment, each class described in the training model will be representative of a predetermined temperature at which point the semiconductor device will be characterized. Additionally, the results of the following experiment will utilize half of the experimental data as a supervised training model for the SVM, with the other half aggregated according to the resultant classifier constructed by the training data.

D. Test Setup

The experimental setup is shown in Fig. 1. A buck converter with a 4.4 mH inductor and a 1.02 mF load capacitor drives a 150 Ω load. The SiC MOSFETs (C3M0065090D) are switched at 20 kHz with a 50% duty cycle. A chassis mounted power resistor is attached to the MOSFET heat sink and used to more effectively control the semiconductor device temperature. Two Line Impedance Stabilization Networks (LISN) monitor EMI in the circuit, feeding frequency data to an MDO3104 oscilloscope/spectrum analyzer.

The drain to source voltage (V_{DS}) of each MOSFET and the voltage at the LISN's measurement terminal were observed to quantify changes in switching speed as junction temperature

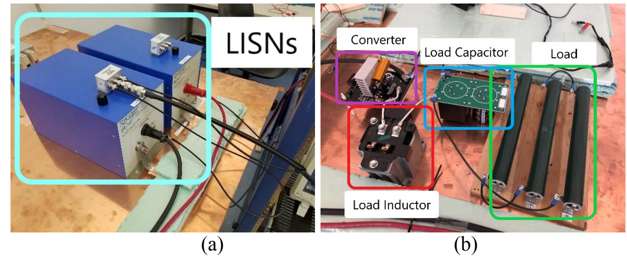

(a) (b)

Fig 1. (a) LISNs used for noise measurement and (b) buck converter with a heating element for the experiments.

increased. Fig. 2 depicts the turn off event of the upper device for four different case temperatures. The switching waveforms at higher temperatures are shown to lead the waveform of lower temperatures, illustrating a reduction in turn-off time as temperature increases. Furthermore, the LISN's voltage shows a higher peak voltage results for the higher operating temperatures. This indicates that the conducted EMI should increase with temperature around the frequencies related to the dv/dt of the device.

Tests were conducted to confirm that the EMI of the circuit reflected these altered switching characteristics. Data collection was organized into three types of noise measurements across two frequency ranges. Common mode noise (CM), differential mode noise (DM), and total noise (TN) were measured at room temperature (~22), 30 , in ten-degree Celsius increments until 60 . At each temperature, the noise spectrum was measured first between 100 kHz and 1 MHz (LF), then at 1 MHz to 40 MHz (HF).

III. Analysis

The test results for total noise (TN) E-PHM measurements are shown in Fig. 3 - 4. The buck converter operated with an input voltage of 270 V, an output voltage of 135 V, and a switching frequency of 20 kHz, yielding a total output power of ~135 W. The plots shown were generated in MATLAB from the mean noise measured in each set of tests. For brevity, measurements are only shown for total noise, though common mode and differential mode noise similarly exhibit distinguishing behavior.

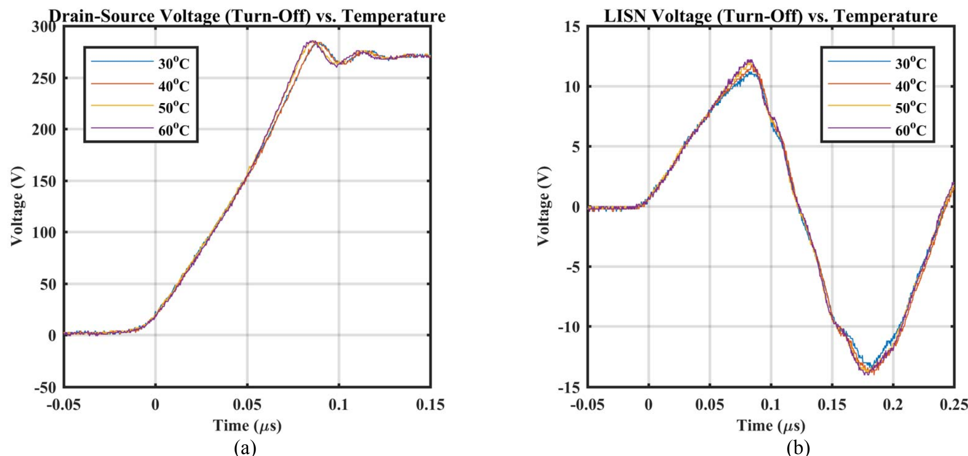

Fig. 2. (a) Drain-source voltage of SiC device measured at different temperatures and (b) LISN voltage versus device during device turn-off window.

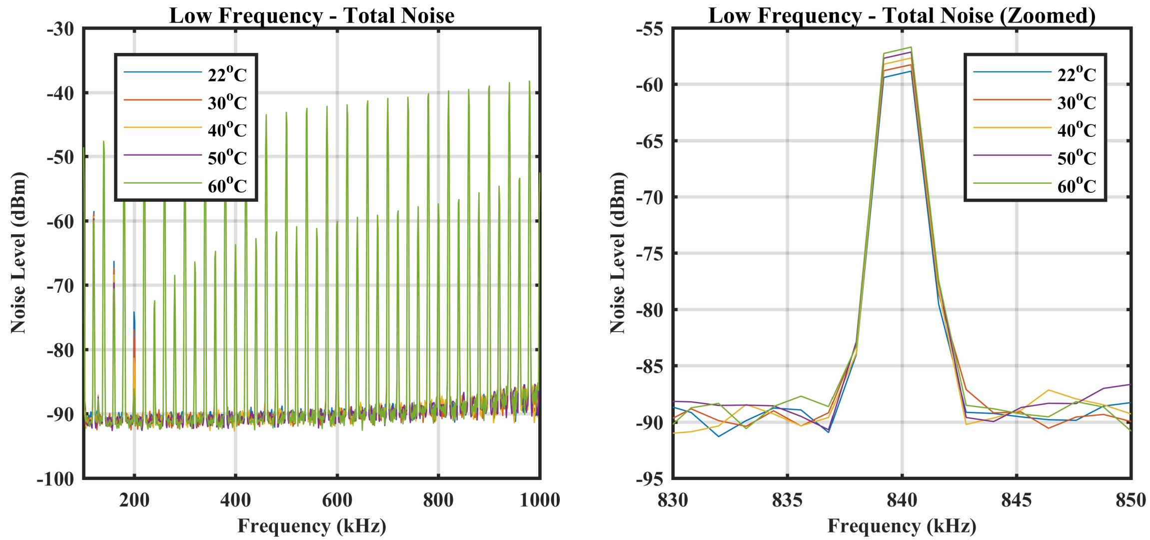

Fig. 3. (a) LF total noise (TN) spectrum of buck converter topology and (b) Zoomed view of LF TN exhibiting higher harmonics at between tested temps.

Immediately, one can observe that the HF measurements yielded results with greater differentiation between temperature tests than the low frequency. Test results in the lower frequency range of 1 kHz to 100 kHz yielded few frequencies in which an outstanding distinction could be made from noise measurements taken at different temperatures (Fig. 3). However, in the higher test frequency range of 1 MHz to 40 MHz, the frequency spectrum 25 MHz to 38 MHz yields a significant stratification between the various temperatures, demonstrating the feasibility for determining MOSFET junction temperature using the frequency spectrum of the circuit's EMI (Fig. 5).

An SVM machine learning model classified the measured data and determined the junction temperature of the MOSFET. Five classes representing each tested temperature were defined for this experiment. A training model was developed using 25 data samples gathered at each MOSFET junction temperature per noise spectrum (TN, CM, & DM). An additional 25 data sets at each temperature were then classified according to the developed model.

Tables I and II depict the resulting confusion matrices of the SVM model using total noise EMI measurements. Across all noise spectrums, the model was able to reliably classify junction temperature with 100% accuracy. This result indicates that a single EMI measurement, the total noise, can be used to implement this approach.

To verify these results, a second iteration of the experiment was executed under the same test conditions, testing at the higher frequency range only (1 MHz to 40 MHz). This subsequent test produced identical results to the first.

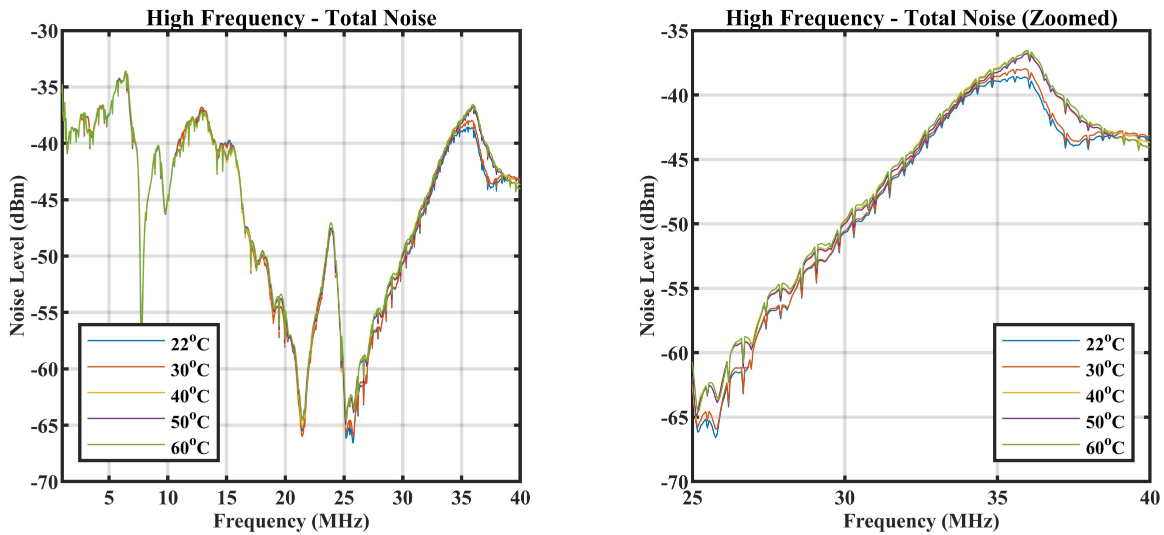

Fig 4. (a) HF spectrum of TN noise at each temperature and (b) Zoomed view of HF TN exhibiting higher noise at evaluated temperatures.

TABLE I. CONFUSION MATRIX FOR LOW FREQUENCY TN E-PHM TEMPERATURE MEASUREMENTS.

Dec. \ Act.	22	30	40	50	60
22	**25**	0	0	0	0
30	0	**25**	0	0	0
40	0	0	**25**	0	0
50	0	0	0	**25**	0
60	0	0	0	0	**25**

TABLE II. CONFUSION MATRIX FOR HIGH FREQUENCY TN E-PHM TEMPERATURE MEASUREMENTS.

Dec. \ Act.	22	30	40	50	60
22	**25**	0	0	0	0
30	0	**25**	0	0	0
40	0	0	**25**	0	0
50	0	0	0	**25**	0
60	0	0	0	0	**25**

TABLE III. CONFUSION MATRIX FOR HIGH FREQUENCY TN E-PHM TEMPERATURE MEASUREMENTS USING ORIGINAL TRAINING MODEL

Dec. \ Act.	22	30	40	50	60
22	**50**	0	0	0	0
30	0	**50**	0	0	0
40	0	0	**50**	0	0
50	0	0	0	**50**	0
60	0	0	0	0	**50**

TABLE IV. CONFUSION MATRIX FOR HIGH FREQUENCY CM E-PHM TEMPERATURE MEASUREMENTS USING ORIGINAL TRAINING MODEL

Dec. \ Act.	22	30	40	50	60
22	**50**	0	0	0	0
30	0	**50**	0	0	0
40	0	0	**50**	0	0
50	0	0	0	**50**	0
60	0	0	0	**1**	**49**

TABLE V. CONFUSION MATRIX FOR HIGH FREQUENCY DM E-PHM TEMPERATURE MEASUREMENTS USING ORIGINAL TRAINING MODEL

Dec. \ Act.	22	30	40	50	60
22	**50**	0	0	0	0
30	0	**50**	0	0	0
40	**1**	0	**49**	0	0
50	0	0	0	**50**	0
60	0	0	0	0	**50**

To affirm the efficacy of the SVM approach, the training model of the first experiment was used to classify all 50 sets of data gathered during the second experiment. The resulting confusion matrices can be seen in Tables III to V. As shown in the table, the SVM maintains its high reliability even when trained with a different generation of data from the same experiment setup. The TN model achieved 100% accuracy while CM and DM produced only one error each for a total of 99.6% accuracy.

IV. CONCLUSION

This paper analyzes the temperature dependent characteristics of semiconductor devices to demonstrate the efficacy of online, real-time analysis of device operation suitable for high temperature safety critical applications. The results demonstrate altered device operational characteristics that can be consistently reproduced in the converter. Additionally, an SVM model was able to reliably predict the MOSFET junction temperature utilizing the distinguishing features in the spectrum, confirming that E-PHM is feasible as an effective monitoring tool. While this original method features the implementation of an SVM algorithm to characterize device operation, further refining the machine learning protocol could produce a more accurate estimation of device temperature with greater resolution. Rather than a classification system, for example, a regression model or artificial neural network would permit the precise approximation of device temperature without relying on the training of a finite selection of classes.

The systems outlined in this paper were performed at voltage levels and device temperatures more than capable of reflecting the environment of modern electric transportation, allowing for a cost-effective and simple solution for prognostic analysis of device health in these industries.

REFERENCES

[1] A. Bryant *et al.*, "Investigation Into IGBT dV/dt During Turn-Off and Its Temperature Dependence," in *IEEE Transactions on Power Electronics*, vol. 26, no. 10, pp. 3019-3031, Oct. 2011.

[2] D. Xiang, L. Ran, P. Tavner, S. Yang, A. Bryant and P. Mawby, "Condition Monitoring Power Module Solder Fatigue Using Inverter Harmonic Identification," in *IEEE Transactions on Power Electronics*, vol. 27, no. 1, pp. 235-247, Jan. 2012.

[3] Y. Avenas, L. Dupont, N. Baker, H. Zara and F. Barruel, "Condition Monitoring: A Decade of Proposed Techniques," in *IEEE Industrial Electronics Magazine*, vol. 9, no. 4, pp. 22-36, Dec. 2015.

[4] M. Boubin, J. P. Doran, W. Guo, Y. Rajasekhar and M. Scott, "EMI Diagnostics of Three Phase Inverters Using Machine Learning Algorithms," 2018 IEEE Energy Conversion Congress and Exposition (ECCE), Portland, OR, 2018, pp. 4062-4069.

[5] S. Yang, D. Xiang, A. Bryant, P. Mawby, L. Ran and P. Tavner, "Condition Monitoring for Device Reliability in Power Electronic Converters: A Review," in *IEEE Transactions on Power Electronics*, vol. 25, no. 11, pp. 2734-2752, Nov. 2010.

[6] S. Pu, E. Ugur, B. Akin and H. Akca, "Investigation of EM radiation changes in SiC based converters throughout device aging," *2017 IEEE 5th Workshop on Wide Bandgap Power Devices and Applications (WiPDA)*, Albuquerque, NM, 2017, pp. 190-194.

[7] Z. Chen, Y. Yao, M. Danilovic and D. Boroyevich, "Performance evaluation of SiC power MOSFETs for high-temperature applications," *2012 15th International Power Electronics and Motion Control Conference (EPE/PEMC)*, Novi Sad, 2012, pp. DS1a.8-1-DS1a.8-9.

[8] Z. Wang, X. Shi, Y. Xue, L. M. Tolbert, B. J. Blalock and F. Wang, "Design and performance evaluation of overcurrent protection schemes for silicon carbide (SiC) power MOSFETs," *2013 IEEE Energy Conversion Congress and Exposition*, Denver, CO, 2013, pp. 5418-5425.

[9] C. M. DiMarino, R. Burgos and B. Dushan, "High-temperature silicon carbide: characterization of state-of-the-art silicon carbide power transistors," in *IEEE Industrial Electronics Magazine*, vol. 9, no. 3, pp. 19-30, Sept. 2015.

[10] K. Loudière, A. Bréard, C. Vollaire, F. Costa, H. Moussa and R. Meuret, "Impact of the temperature of a power module on conducted EMI emitted by a buck converter," *2016 IEEE International Symposium on Electromagnetic Compatibility (EMC)*, Ottawa, ON, 2016, pp. 604-609.

[11] J. Qi *et al*., "Dynamic performance of 4H-SiC power MOSFETs and Si IGBTs over wide temperature range," *2018 IEEE Applied Power Electronics Conference and Exposition (APEC)*, San Antonio, TX, 2018, pp. 2712-2716.

[12] S. L. Rumyantsev, M. S. Shur, M. E. Levinshtein, P. A. Ivanov, J. W. Palmour, A. K. Agarwal, B.A. Hull and S. H. Ryu, “Channel mobility and on-resistance of vertical double implanted 4H-SiC MOSFETs at elevated temperatures,” Semiconductor Science & Technology, vol. 24, pp. 075011-6, 2009.

[13] H. Niu and R. D. Lorenz, "Sensing power MOSFET junction temperature using gate drive turn-on current transient properties," *2014 IEEE Energy Conversion Congress and Exposition (ECCE)*, Pittsburgh, PA, 2014, pp. 2909-2916.

[14] A. I. Belousov, S. A. Verzakov, and J. V. Frese, “Applicational aspects of support vector machines,” *Journal of Chemometrics*, vol. 16, no. 8-10, pp. 482–489, Aug. 2002.